Deletion of the mitochondrial matrix protein cyclophilin-D prevents parvalbumin interneuron dysfunction and cognitive deficits in a mouse model of NMDA hypofunction

Aarron Phensy[1], Kathy L. Lindquist[1], Karen A. Lindquist[1], Dania Bairuty[1], Esha Gauba[2], Lan Guo[2], Jing Tian[2], Heng Du[2], and Sven Kroener[1]

Abbreviated title: CypD deletion reduces oxidative stress in PVI

[1] School of Behavioral and Brain Sciences, The University of Texas at Dallas, Richardson, TX 75080

[2] Department of Biological Sciences, The University of Texas at Dallas, Richardson, TX 75080

Correspondence should be addressed to:
Sven Kroener, PhD
School of Behavioral and Brain Sciences,
The University of Texas at Dallas,
800 West Campbell Rd, BSB14
Richardson, TX 75080
Email: kroener@utdallas.edu
Phone: 972-883-2039
Fax: 972-883- 3491

Number of pages: 24

Number of figures: 6

Number of tables: 0

Number of multimedia: 0

Number of words in the abstract: 217

Number of words in the introduction: 648

Number of words in the discussion: 1499

Author contributions: AP, HD, and SK designed the research; AP, KLL, KAL, DB, EG, LG, JT, HD, and SK performed research; AP, LG, HD, and SK analyzed data; AP and SK wrote the paper.

Conflict of Interest: The authors report no conflict of interest.

Funding sources: AP is supported by NIH (F31MH118883). SK wishes to acknowledge support from The University of Texas at Dallas and NIH (R01AG053588). HD is supported by NIH (R01AG053588; R00AG037716).

Abstract

Redox dysregulation and oxidative stress are final common pathways in the pathophysiology of a variety of psychiatric disorders, including schizophrenia. Oxidative stress causes dysfunction of GABAergic parvalbumin-positive interneurons (PVI), which are crucial for the coordination of neuronal synchrony during sensory- and cognitive-processing. Mitochondria are the main source of reactive oxygen species (ROS) in neurons and they control synaptic activity through their roles in energy production and intracellular calcium homeostasis. We have previously shown that in male mice transient blockade of NMDA receptors during development (subcutaneous injections of 30 mg/kg ketamine (KET) on postnatal days 7, 9, and 11) results in long-lasting alterations in synaptic transmission and reduced parvalbumin expression in the adult prefrontal cortex (PFC), contributing to a behavioral phenotype that mimics multiple symptoms associated with schizophrenia. These changes correlate with oxidative stress and impaired mitochondrial function in both PVI and pyramidal cells. Here, we show that genetic deletion (*Ppif*$^{-/-}$) of the mitochondrial matrix protein cyclophilin D (CypD) prevents perinatal KET-induced increases in ROS and the resulting deficits in PVI function, and changes in excitatory and inhibitory synaptic transmission in the PFC. Deletion of CypD also prevented KET-induced behavioral deficits in cognitive flexibility, social interaction, and novel object recognition. Taken together, these data highlight how mitochondrial activity may play an integral role in modulating PVI-mediated cognitive processes.

Significance Statement

Mitochondria are important modulators of oxidative stress and cell function, yet how mitochondrial dysfunction affects cell activity and synaptic transmission in psychiatric illnesses is not well understood. NMDA receptor blockade with ketamine during development causes oxidative stress, dysfunction of parvalbumin-positive interneurons (PVI), and long-lasting physiological and behavioral changes. Here we show that mice deficient for the mitochondrial matrix protein cyclophilin D show robust protection from PVI dysfunction following perinatal NMDAR-blockade. Mitochondria serve as an essential node for a number of stress-induced signaling pathways and our experiments suggest that failure of mitochondrial redox regulation can contribute to PVI dysfunction.

Introduction

Schizophrenia is a neurodevelopmental disorder in which genetic risk factors and early life stressors converge (Harrison and Owen, 2003). Genes involved in glutamatergic synaptic transmission figure prominently among both the rare (Timms et al., 2013; Pocklington et al., 2015; Sekar et al., 2016) and common (Pers et al., 2016) gene variants that contribute to the heritable risk for schizophrenia. In the frontal cortex, these genes are highly expressed early in development (Gulsuner et al., 2013; Birnbaum et al., 2015). Dysfunction of glutamatergic NMDARs during neurodevelopment can disrupt maturation of interneurons (Zhang and Sun, 2011) and cause abnormalities in the GABAergic and dopaminergic systems in schizophrenia (Olney et al., 1999; Krystal et al., 2002; Catts et al., 2013). Aberrant NMDAR activity can therefore shift the cortical excitation-inhibition (E/I) balance (Insel, 2010; Lewis et al., 2012), leading to increased basal neural activity (Jadi et al., 2016), excessive glutamatergic release (Plitman et al., 2014), and oxidative stress (Hardingham and Do, 2016; Steullet et al., 2016). In support of this, NMDAR antagonists such as phencyclidine and ketamine (KET) induce a schizophrenia-like syndrome in healthy subjects, and exacerbate symptoms in schizophrenic patients (Malhotra et al., 1997; Krystal et al., 2002; Anticevic et al., 2012). Pharmacological blockade or genetic deletion of NMDARs in rodents mimics many of the behavioral symptoms seen in patients with schizophrenia, and it also reduces markers of GABAergic interneurons, including cells that express the calcium-binding protein parvalbumin (Abekawa et al., 2007; Braun et al., 2007; Belforte et al., 2010). Reductions in parvalbumin expression are a core finding of post-mortem studies in schizophrenia patients (Olney et al., 1999; Lewis et al., 2005; Akbarian and Huang, 2006) that is replicated by virtually all animal models of the disease (Jiang et al., 2013; Steullet et al., 2017). Fast-spiking PVI have a unique metabolic profile that is reflected in a large number of mitochondria and enriched cytochrome c oxidase (Kann and Kovacs, 2007), which seems to make them particularly susceptible to external stressors during development (Hardingham and Do, 2016; Steullet et al., 2017).

Mitochondria are crucial regulators of oxidative and nitrosative stress (Chen et al., 2003; Li et al., 2004), and transcriptomic, proteomic, and metabolomic studies in post-mortem samples from subjects with schizophrenia indicate alterations in the expression of several proteins associated with mitochondrial function (Prabakaran et al., 2004; Altar et al., 2005; Iwamoto et al., 2005; Hjelm et al., 2015). Altered levels of ATP and mitochondrial dysfunction in the frontal lobe are correlated with negative symptoms, as well as cognitive and memory deficits in schizophrenia (Ben-Shachar and Laifenfeld, 2004; Rajasekaran et al., 2015). Oxidative and other cellular stresses promote translocation of the mitochondrial matrix protein cyclophilin D (CypD) to the inner membrane. This translocation triggers the opening of the mitochondrial permeability transition pore (mPTP) (Connern and Halestrap, 1994; Baines et al., 2005), which is important in glutamate excitotoxicity that results from overactivation of glutamate receptors and subsequent excessive calcium entry into the cell (Schinder et al., 1996; White and Reynolds, 1996). Prolonged CypD-mediated opening of mPTP causes collapsed mitochondrial membrane potential, elevated mitochondrial ROS generation, and lowered ATP production, leading to metabolic changes and ultimately cell death (Basso et al., 2005; Halestrap, 2010). Because CypD is a necessary component of the mPTP, reducing CypD translocation in order to block mPTP formation can preserve mitochondrial function (Du and Yan, 2010).

Here, we investigated whether genetic deletion of CypD (*Ppif*$^{-/-}$) can prevent changes in PVI function, PFC physiology, and behavior that develop in a well-characterized rodent model of NMDA hypofunction. Perinatal treatment with ketamine induced oxidative stress and reduced PV expression in the PFC of wildtype- but not of *Ppif*$^{-/-}$ mice. CypD-deletion similarly protected against changes in glutamatergic transmission at PVI and deficits in cognitive flexibility, social interaction, and novel object recognition. These data indicate that mitochondrial redox regulation is an important contributor to PVI dysfunction and the resulting E/I imbalance that results from NMDAR-hypofunction.

Materials and Methods

Transgenic *Ppif*$^{-/-}$ mice: Cyclophilin-D knockout mice (B6;129-*Ppif*^{tm1Jmol}/J; The Jackson Laboratory; RRID:IMSR_JAX:009071), were crossed with G42 mice (CB6-Tg[Gad1-EGFP]G42Zjh/J; The Jackson Laboratory; RRID:IMSR_JAX:007677) which express GFP in PVI neurons, in order to identify PV+ neurons in slice electrophysiology experiments. First- and second-generation breeders were selected and their WT (CB6-TgWT; Gad1-EGFP) and *Ppif*$^{-/-}$ (CB6-Tg*Ppif*$^{-/-}$; Gad1-EGFP) offspring were used for experiments. All procedures were approved by the Institutional Animal Care and Use Committee of The University of Texas at Dallas.

Perinatal ketamine treatment: On postnatal day 7, 9, and 11 mice received subcutaneous injections of either saline or a sub-anesthetic dose of the NMDA-antagonist ketamine (30mg/kg; Ketathesia HCL, Henry Schein). Both *Ppif*$^{-/-}$ and WT mice received either perinatal ketamine (KET) or saline injections, creating four groups: Wild type mice that received saline injections (WT-SAL); Wild type mice that received ketamine injections (WT-KET); *Ppif*$^{-/-}$ mice that received saline injections (*Ppif*$^{-/-}$-SAL); and *Ppif*$^{-/-}$ mice that received ketamine treatment (*Ppif*$^{-/-}$-KET). All experiments were performed on adult male *Ppif*$^{-/-}$ and WT mice (60-120 days old). Animals that participated in behavioral experiments were handled for 5 minutes a day in the vivarium for 2 weeks prior to the test and then also in the room in which behavioral testing took place for 3 days prior to the test. On the day of testing, animals were transferred to the behavioral room at least 30 min before testing began. Behavioral testing and analysis was performed by experimenters blind to the experimental condition of the subjects.

Immunohistochemistry: Animals were perfused transcardially with saline for 2 minutes, followed by 4% paraformaldehyde in 0.12 M phosphate-buffered saline (PBS), at 4°C, pH 7.4; Fisher Scientific) for 10 minutes using a peristaltic pump (5.5 ml/min; PeriStar Pro, WPI). Brains were post-fixated in paraformaldehyde with 30% sucrose for 1 h and then transferred to 30% sucrose in PBS for 18 h at 4°C. Coronal slices (40 um) were cut on a freezing microtome. Free-floating sections were incubated in rabbit anti-parvalbumin (1:2000 working dilution; Swant Cat# PV 25, RRID:AB_10000344) in PBS and 0.3% Triton X (Sigma-Aldrich) for 36 h at 4°C. Sections were washed three times for 10 min each in PBS before they were incubated in secondary 594 goat anti-rabbit (1:1000 working dilution; Jackson ImmunoResearch Labs Cat# 111-585-144, RRID:AB_2307325) in PBS and 0.3% Triton X. Sections were washed, mounted, and cover slipped using Prolong Gold Antifade with DAPI (Thermo Fisher Scientific). To quantify PVI immunofluorescence a minimum of four sections from each animal containing the prelimbic and infralimbic regions of the PFC were imaged on a confocal microscope (FluoView 1000, Olympus) at 20x magnification. The number of PV+ cells were hand counted in ImageJ (National Institutes of Health), and DAPI-labeled cells were counted using the thresholding function in ImageJ to obtain the percentage of total PV+ cells among all DAPI-labeled cells. In order to quantify 4-Hydroxynonenal (4-HNE) levels in PVI free-floating sections were incubated in rabbit anti-parvalbumin (1:2000 working dilution; Swant Cat# PV 25, RRID:AB_10000344) and mouse anti-4HNE (1:1000 working dilution; Abcam Cat# ab48506, RRID:AB_867452) in PBS and 0.3% Triton X (Sigma-Aldrich) for 36 h at 4°C. Sections were washed three times for 10 min each in PBS before they were incubated in secondary 488 goat anti-rabbit (1:1000 working dilution; Jackson ImmunoResearch Labs Cat# 111-095-144, RRID:AB_2337978) and

647 goat anti-mouse (1:500 working dilution; Cell Signaling Technology Cat# 4410, RRID:AB_1904023) in PBS and 0.3% Triton X. To quantify 4HNE in PVI cells PVI immunofluorescence confocal images (20x magnification) from three sections of the prelimbic and infralimbic cortex were taken for each animal. ROIs were drawn around all PV+ cells in cellSens (Olympus cellSens Software, RRID:SCR_016238) and the mean gray intensity of the 4HNE signal for each cell was selected and averaged across each image and then across all three slices for every animal.

GSH:GSSG Assay: In order to measure the ratio between reduced glutathione (GSH) and oxidized glutathione (GSSG), GSH, GSSG, and total glutathione were measured following the manufacturer instructions (glutathione detection kit, catalog #ADI-900-160, Enzo Life Sciences). In brief, animals were killed and the medial PFC containing the infralimbic and prelimbic cortex was dissected and homogenized in ice-cold 5% (w/v) meta-phosphoric acid (20 ml/g tissue), followed by centrifugation at 12,000 x g for 10 min at 4C. The resultant supernatant was collected for glutathione detection. For the measurement of GSSG and total glutathione, 2 M 4-vinylpyridine was added to the samples at a dilution of 1:50 (v/v). The samples were then incubated for 1 h at room temperature to derivatize reduced glutathione. Afterward, the samples were diluted in the reaction mix buffer. The reaction was observed by immediately and continuously recording changes at an optical density of 405 nm by using a microplate reader (Biotek) for a total of 15 min at 1 min intervals. The concentrations of total, oxidized, and reduced glutathione were normalized to the original wet weight of the tissue.

Electrophysiology: Electrophysiological experiments used GFP+ hemizygous mice. Mice were anesthetized with urethane (3 g/kg body weight; Fisher Scientific) and transcardially perfused for one minute with gravity-fed ice-cold oxygenated (95% O2. 5% CO2) cutting ACSF, consisting of (in mM): 110 choline (Sigma-Aldrich), 25 NaHCO3 (Fisher Scientific), 1.25 NaH2PO4 (Fisher Scientific), 2.5 KCl (Sigma-Aldrich), 7 MgCl2 (Sigma-Aldrich), 0.5 CaCl2 (Sigma-Aldrich), 10 dextrose (Fisher Scientific), 1.3 L-ascorbic acid (Fisher Scientific), and 2.4 Na+- pyruvate (Sigma-Aldrich). Immediately after, brains were extracted and coronal sections (350 um) of the frontal cortex were cut on a vibratome (VT1000S, Leica) in cutting ACSF. Slices were transferred into a holding chamber containing warmed (35C) recording ACSF and cooled to room temperature over a one-hour period. The recording ACSF consisted of (in mM): 126 NaCl (Fisher Scientific), 25 NaHCO3, 1.25 NaH2PO4, 2.5 KCl, 2 MgCl2, 2 CaCl2, 10 dextrose, 2.4 Na+-pyruvate, and 1.3 L-ascorbic acid. For data collection, slices were transferred to a recording chamber affixed to an Olympus BX61WI microscope (Olympus) with continuous perfusion of oxygenated recording ACSF at room temperature. Whole-cell voltage-clamp recordings were obtained from pyramidal cells and PVIs in the prelimbic and infralimbic cortex using an Axon Multiclamp 700B amplifier (Molecular Devices). Data were acquired and analyzed using AxoGraph X (AxoGraph Scientific). Recording electrodes (WPI; 3–5 MΩ open tip resistance for pyramidal cells, 6–8 MΩ for interneurons) were filled with an internal solution consisting of (in mM): 130 CsCl (Sigma-Aldrich), 20 tetraethylammonium chloride (Sigma-Aldrich), 10 HEPES (Sigma-Aldrich), 2 MgCl2, 0.5 EGTA (Sigma-Aldrich), 4 Mg2+-ATP (Sigma-Aldrich), 0.3 Lithium-GTP (Sigma-Aldrich), 14 phosphocreatine (Sigma-Aldrich), and 2 QX-314 bromide (Tocris Bioscience). Theta-glass pipettes (Warner Instruments) connected to a stimulus isolator (WPI) were used for focal stimulation of synaptic potentials. Access resistance was

monitored throughout the recording, and a <20% change was deemed acceptable. Spontaneous EPSCs were isolated by blocking chloride channels with the addition of picrotoxin (75uM; Sigma-Aldrich) into the recording ACSF. Spontaneous IPSCs were isolated by blocking AMPA receptor-mediated events with CNQX (6-cyano-7-nitroquinoxaline-2,3-dione; 20uM; Sigma-Aldrich). Miniature events were isolated by blocking sodium channels with the addition of tetrodotoxin (1uM; Alomone Labs). The frequency and amplitude of events were measured from 200 s of continuous recording using MiniAnalysis (Synaptosoft) with a threshold set at two times the RMS baseline noise. The ratio of currents through NMDA or AMPA receptors, respectively, was obtained by clamping cells at +40mv holding potential and applying local electrical stimulation. A compound evoked EPSC (eEPSC) was first recorded, then the AMPA component was isolated by washing CPP ((+/-)-3-(2-carboxypiperazin-4-yl)propyl-1-phosphonic acid; 10 uM; Sigma-Aldrich) into the bath. A minimum of 15 sweeps each were average for the compound and AMPA-only eEPSCs. The NMDA component was then obtained by digital subtraction of the AMPA component from the compound trace. The peak amplitude of the NMDA and AMPA traces were used to calculate the NMDAR/AMPAR ratio.

Rule-Shifting: Procedures for our rule-shifting task followed those previously described (Phensy et al., 2017b). Mice were food restricted to 85% of their free-feeding weight over two weeks and handled for at least 5 minutes a day. Testing took place in white wooden plus maze (each arm is 10x34x15 cm, with a 10x10 cm center area) under low ambient illumination. The arms were labeled East, West, South, and North for reference. On days 4-6, the maze was converted into a T-maze by blocking off one of the arms with a divider, and additionally a visual cue (vertical black and white stripes on a 13x10 cm plastic sheet) was placed alternately near the entrance of one of the two choice arms in a pseudorandom manner (see below). During all days, reward pellets (Cheerio bits) were placed around the outside of the maze in order to prevent animals from using olfactory cues to infer the location of the reward. Mice were habituated to the maze over three days. On the first day of habituation, 4 reward pellets (1/8th Cheerios bits) were placed in each of the arms of the plus maze. Animals were placed into the center of the maze and were allowed to freely explore the maze for 15 minutes. If a mouse consumed all 16 pellets before the end of the habituation period, it was briefly placed in a holding cage while the maze was rebaited, and then the mouse was placed back into the maze until the end of the 15-minute period. On the second day of habituation, arms were baited with two pellets each, and on the third day of habituation only one food pellet was placed at the end of each arm. To reach habituation criterion, animals were required to consume all 4 food pellets at least 4 times within the 15-minute period. All animals in this study reached this criterion on the third habituation day. On the following day (Day 4), the plus maze was converted into a T-maze by blocking off one of the arms and the animals' turn bias was determined. Therefore, mice were placed in the stem arm and allowed to turn left or right to obtain a food pellet. After the mouse consumed the reward, it was returned to the stem arm and allowed to make another choice. If the mouse chose the same arm as on the initial choice, it was returned to the stem arm until it chose the other arm and consumed the food pellet. Once both food pellets were consumed the maze was rebaited and the next trial began. The direction of the initial turn chosen four or more times over seven trials was considered the turn bias. On the next day (Day 5, Response Discrimination), mice were trained on an egocentric task which required them to always turn towards one side (left or right, chosen opposite to the direction of their turn bias) to obtain the food reward. The

location of the stem arm was pseudorandomly rotated among 3 arms (East, West, and South) to discourage mice from using an allocentric spatial strategy. During all trials a visual cue was placed close to the entrance of one of the choice arms. Placement of this cue into the right or left arm varied pseudorandomly to balance the frequency of occurrences in each arm across blocks of 12 consecutive trials. Similarly, the order of the stem arms alternated pseudorandomly in a balanced fashion across blocks of 12 trials. Training continued until the mouse made 9 correct choices over 10 consecutive trials. When animals achieved this acquisition criterion, a probe trial was administered. In the probe trial the previously unused fourth arm (North) was used as a stem arm. If the mice performed the probe trial correctly, Response Discrimination training was completed. If an incorrect turn occurred, response training continued until the mouse made another five consecutive correct choices, and then another probe trial was administered. On the next day (Day 6, Shift-to-Visual-Cue Discrimination), mice were trained to shift their strategy to now select the choice arm with the visual cue in order to obtain food rewards. The location of the visual cue and the position of the start arm were again varied pseudorandomly so that their frequency was balanced across blocks of 12 consecutive trials. The training and response criteria for the Shift-to-Visual-Cue Discrimination were identical to those during Response Discrimination. Performance and Error Analysis: For each of the two test days we analyzed the total number of trials to criterion and the number of probe trials required to reach criterion. For the Shift-to-Visual-Cue Discrimination, errors were scored as entries into arms that did not contain the visual cue, and they were further broken down into three subcategories to determine whether the animals' treatment altered the ability to either shift from the previously learned strategy (perseverative errors), or to maintain the new strategy after perseveration had ceased (regressive errors, or never-reinforced errors). In order to detect shifts in the strategies that animals used, trials were separated into consecutive blocks of four trials each. A perseverative error occurred when a mouse made the same egocentric response as required during the Response Discrimination, but which was opposite to the direction of the arm containing the visual cue. Six of every 12 consecutive trials required the mouse to respond in this manner. A perseverative error was scored when the mouse entered the incorrect arm on three or more trials per block of 4 trials. Once the mouse made less than three perseverative errors in a block, all subsequent errors of the same type were now scored as regressive errors (because at this point the mouse was following an alternative strategy at least half of the time). So-called never-reinforced errors were scored when a mouse entered the incorrect arm on trials where the visual cue was placed on the same side that the mouse had been trained to enter on the previous day.

Novel Object Recognition: Testing was conducted in a white wooden open chamber (39 x 19 x 30.5 cm) and sessions were recorded from above by a web camera for later analysis. Wooden toys (approximately 3 x 5 cm) were used as stimulus objects and pseudorandomly selected as either the familiar or novel objects. In addition, in a different cohort of mice object preference was measured prior to experiments to ensure mice showed no inherent preference across the objects used. Mice were first habituated for 10 minutes on two consecutive days to the empty chamber. On the third day mice were again habituated for 10 minutes before the training and test trials begun. Therefore, mice were placed in their home cage while the chamber was cleaned and two objects were placed inside the chamber. Mice were then placed inside the chamber and allowed to investigate the two objects for 3 minutes before being placed back into

the home cage for a 2-minute intertrial interval during which one of the two familiar objects was replaced with a novel object. After 2 minutes mice were placed back into the chamber and allowed to explore both the familiar and novel object for an additional 2 minutes. The objects were cleaned with 20% ethanol and the chamber was cleaned with 70% ethanol between animals. The amount of time the mice spent investigating the objects during both the training trial and the novel object trial were analyzed. In order to assess whether animals recognized the novel object as such we calculated a "recognition index", which is the percentage of time spent investigating the novel object over the total investigation time for both objects.

Social Interaction: Experimental mice and two size- and age-matched stimulus mice were housed individually for three days prior to the task. On the day of the test, the experimental mouse was placed into a new cage with 2.5 grams of their original bedding material to allow the animal to habituate for one hour. Stimulus mice were kept in a small custom cylindrical holding apparatus (height 20 cm, steel bars separated by 1 cm, acrylic base and lid), which could be placed inside the test cage. After one hour, the first stimulus mouse was placed in the holding apparatus and positioned into the cage with the test mouse for a trial interval of 1-minute while being recorded by an overhead camera. This was repeated for four trials with an intertrial interval of 10 minutes (Trials 1-4). On the fifth trial, a novel stimulus mouse was introduced into the cage to test for social recognition memory. All trials were recorded via an overhead camera and the interaction times (defined as sniffing and investigation of the stimulus mouse at close proximity) were analyzed for each trial.

Statistical Analysis: Differences between groups were compared using one-way ANOVAs or two-way mixed ANOVAs as indicated. Post-hoc analyses using Tukey correction were used to determine specific group differences. All data is presented as mean ± standard error of the mean (SEM). An alpha level of $p < 0.05$ was considered significant.

Results

Perinatal KET-treatment reduces parvalbumin expression in adult mPFC in WT, but not in *Ppif*$^{-/-}$ mice

A reduction in the number of parvalbumin-expressing interneurons (PVI) is a hallmark of schizophrenia (Lewis et al., 2005; Nakazawa et al., 2012) that is recapitulated by most animal models, including perinatal KET application (Jeevakumar et al., 2015; Phensy et al., 2017a). To determine if genetic deletion of Cyclophilin D can protect against KET-induced reductions in PVI, we performed immunohistochemistry and quantified the number of parvalbumin+ somata in the mPFC from both adult WT and *Ppif*$^{-/-}$ mice which received either KET or saline during development (Fig. 1). A one-way ANOVA revealed a main effect of treatment on the number of PV+ cells over the number of DAPI+ cells ($F_{(3, 30)} = 8.990$, $p < 0.001$). Wildtype KET-treated mice showed a significant loss in PV expression. In contrast, *Ppif*$^{-/-}$-KET mice were protected against KET-induced PVI loss and had similar numbers of PV+ cells than saline-control mice (Fig. 1B).

Ketamine-induced oxidative stress is reduced in *Ppif*$^{-/-}$ mice

Perinatal ketamine treatment leads to long-lasting increases in oxidative stress in adult animals, and PVI are particularly sensitive to redox dysregulation (Do et al., 2009; Phensy et al., 2017a). The ratio between the bioavailable reduced (GSH) and unavailable oxidized (GSSG) forms of the endogenous antioxidant glutathione provides a measure of redox balance in cells. A decrease in this ratio indicates a disruption in redox balance and subsequent oxidative stress. To determine if genetic deletion of cyclophilin D prevents KET-induced oxidative stress, we first measured levels of GSH and GSSG in mPFC tissue taken from adult mice (Fig. 2). A one-way ANOVA revealed that while there was no effect of treatment on total glutathione levels ($F_{(3, 14)} = 1.172$, $p = 0.3556$; Fig. 2A), there was a main effect of treatment on the ratio of GSH / GSSG ($F_{(3, 35)} = 6.664$, $p = 0.001$; Fig. 2B), with WT-KET mice having a significantly reduced GSH / GSSG ratio, indicating increased oxidative stress in these animals. A similar reduction was not observed in *Ppif*$^{-/-}$-KET mice. Next, we measured 4-HNE levels in PVI of the mPFC (Fig. 3). 4-HNE levels increase during periods of oxidative stress due to lipid peroxidation. We colocalized immunofluorescence signals of 4-HNE and parvalbumin to measure changes in 4-HNE specifically in PVI. A one-way ANOVA revealed a main effect of treatment on the mean grey intensity of 4-HNE in PVI ($F_{(3, 27)} = 5.084$, $p = 0.0064$; Fig. 3B). This effect was due to a significant increase in 4-HNE signal in WT-KET mice, which was not present in *Ppif*$^{-/-}$-KET or saline-control mice. Taken together, these results show that PVI in the mPFC of *Ppif*$^{-/-}$ mice are protected from KET-induced oxidative stress.

Perinatal KET-treatment alters inhibitory synaptic transmission onto layer 2/3 mPFC pyramidal cells in WT, but not *Ppif*$^{-/-}$ mice

GABAergic PVI inhibit nearby pyramidal neurons and regulate synchronized firing (Sohal and Rubenstein, 2019). Loss of PVI function leads to reduced GABAergic activity onto pyramidal neurons resulting in disinhibited circuits. In order to determine if CypD deletion prevents KET-induced disinhibition of pyramidal cells, we performed whole cell patch-clamp recordings in layer 2/3 pyramidal neurons of the mPFC and quantified the frequency and amplitude of both spontaneous (sIPSCs) and miniature inhibitory postsynaptic currents (mIPSCs) (Fig. 4). We

found a significant main effect of treatment on the frequency of mIPSCs ($F_{(3, 28)} = 6.547$, p = 0.002; Fig. 4C), but no effect on amplitude ($F_{(3, 28)} = 1.689$, p = 0.192; Fig. 4C). Post-hoc analyses revealed that this was driven by a selective decrease in mIPSC frequency in WT-KET mice. Similar changes did not occur in *Ppif*$^{-/-}$-KET or saline-control mice. KET-treatment did not alter the frequency ($F_{(3, 22)} = 0.8743$, p = 0.469; Fig. 4F) or the amplitude ($F_{(3, 22)} = 1.289$, p = 0.303; Fig. 4F) of sIPSCs. These data suggest that KET reduces GABA release and that this can be prevented by CypD deletion.

KET-treatment induces NMDAR hypofunction in layer 2/3 PVI from WT, but not *Ppif*$^{-/-}$ mice

NMDAR hypofunction likely contributes to aberrant network activity in schizophrenia (Snyder and Gao, 2013). Perinatal KET treatment disrupts PVI development in the mPFC, causing NMDAR hypofunction in adult layer 2/3 PVI (Jeevakumar and Kroener, 2016; Phensy et al., 2017a). In order to test whether CypD deletion can prevent KET-induced changes in NMDAR-signaling we next measured NMDAR and AMPAR currents in GFP+ PVI (Fig. 5A-B). A one-way ANOVA ($F_{(3, 18)} = 4.280$, p = 0.019; Fig. 5B) revealed a main effect of treatment on the ratio of NMDAR:AMPAR currents at layer 2/3 PVI. Consistent with our previous reports (Jeevakumar and Kroener, 2016; Phensy et al., 2017a), WT-KET mice had significantly reduced NMDAR:AMPAR ratios. In contrast, *Ppif*$^{-/-}$-KET mice showed current ratios comparable to saline-treated controls, suggesting that genetic deletion of CypD offers protection from KET-induced aberrant NMDAR signaling in layer 2/3 PVI.

KET-treatment alters spontaneous glutamate release onto layer 2/3 PVI from WT, but not *Ppif*$^{-/-}$ mice

The KET-induced NMDAR hypofunction in layer 2/3 PVI is accompanied by disinhibition of pyramidal cells (as seen in Fig. 4), which subsequently causes increased glutamate release back onto PVI (Jeevakumar and Kroener, 2016; Phensy et al., 2017a). The increased activation of postsynaptic glutamate receptors may lead to excessive calcium influx and contribute to persistent mitochondrial stress in PVI (Phensy et al., 2017a). To further test if CypD deletion prevents KET-induced alterations in glutamatergic signaling at PVI, we recorded spontaneous excitatory postsynaptic currents (sEPSCs) in GFP+ PVI (Fig. 5C-D). A one-way ANOVA revealed a main effect of treatment on sEPSC frequency ($F_{(3, 23)} = 5.812$, p = 0.004; Fig. 5D), without significant changes in sEPSC amplitude ($F_{(3, 20)} = 2.828$, p = 0.065; Fig. 5D). Consistent with the idea that mPFC pyramidal cells from KET-treated mice are disinhibited, post-hoc analyses showed a selective increase in sEPSC frequency in PVI from WT-KET mice; a change that was not seen in any of the other treatment groups.

KET-treatment induces deficits in cognitive flexibility, novel object recognition, and social interactions in WT, but not in *Ppif*$^{-/-}$ mice

In order to determine the functional impact of the physiological changes that result from KET-treatment and CypD deletion, we tested adult mice in a battery of behavioral tasks. These tasks included a rule-shifting task to measure cognitive flexibility, a novel object recognition task which measures (short-term) memory for objects, and a social interaction task which tests deficits in social interaction and novelty discrimination (Fig. 6) (Jeevakumar et al., 2015; Phensy et al., 2017b).

363 Rule Shifting Task

364 Cognitive flexibility is the ability to inhibit the use of a defunct strategy and enable the learning of
365 a new functional strategy. The PFC is important for the ability to shift between strategies, and
366 dysfunctions of the PFC lead to perseveration on inappropriate responses. To examine if CypD
367 deletion protects against KET-induced deficits in cognitive flexibility, we tested WT and *Ppif*$^{-/-}$
368 mice on a well-characterized rule-shifting task that is highly dependent on the mPFC (Birrell and
369 Brown, 2000; Floresco and Magyar, 2006; Young et al., 2009; Hu et al., 2015; Jeevakumar and
370 Kroener, 2016). Mice first learn an egocentric Response Discrimination strategy and then need
371 to shift to a Visual-Cue Discrimination strategy. Mice in all treatment groups reached criterion for
372 the Response Discrimination in the same number of trials ($F_{(3, 26)} = 0.4760$, $p = 0.702$; Fig. 6B).
373 In contrast, a one-way ANOVA showed a main effect of treatment on the number of trials
374 needed to reach criterion during the Shift-to-Visual Cue Discrimination phase of the task ($F_{(3, 26)}$
375 $= 9.576$, $p < 0.001$; Fig. 6B). WT-KET mice took significantly more trials to reach criterion
376 compared to mice in all other treatment groups. To further differentiate the effects of KET-
377 treatment and CypD deletion on cognitive strategies, we analyzed the types of errors
378 (perseverative, regressive, or never-reinforced) that mice committed. A one-way ANOVA ($F_{(3, 26)}$
379 $= 4.361$, $p = 0.013$; Fig. 6C) revealed that KET-treatment caused significantly more overall
380 errors in WT, but not *Ppif*$^{-/-}$ or saline-control mice. Furthermore, there was a significant effect of
381 treatment on perseverative errors ($F_{(3, 26)} = 3.152$, $p = 0.042$; Fig. 6C), but not on regressive ($F_{(3,}$
382 $_{26)} = 1.867$, $p = 0.160$; Fig. 6C), or never-reinforced errors ($F_{(3, 26)} = 0.7296$, $p = 0.544$; Fig. 6C).
383 The significant effect on perseverative errors was due to a selective increase in the WT–KET
384 mice which was not observed in KET-treated *Ppif*$^{-/-}$ or saline-control mice.

385 Novel Object Recognition

386 Mice, like humans, show preference for novel objects and spend more time investigating a novel
387 object if they can correctly distinguish it from a previously encountered object. We next
388 measured how KET treatment and CypD deletion affect novel object recognition (Fig. 6D-E).
389 Preference for the novel object can be calculated as a recognition index, which is the time spent
390 investigating the novel object as a percent of total time investigating both objects. A one-way
391 ANOVA across treatment groups ($F_{(3, 31)} = 6.375$, $p = 0.002$; Fig. 6E) revealed a main effect of
392 treatment on recognition index. WT-KET mice had reduced recognition indices; in contrast, *Ppif*
393 $^{-/-}$-KET exhibited normal novel object recognition and spent similar amounts of time as saline-
394 controls investigating the novel object.

395 Social Interaction

396 Deficits in social cognition and interaction greatly impact the quality of life of patients with
397 schizophrenia. KET-treated mice show reduced social interactions (Jeevakumar et al., 2015;
398 Phensy et al., 2017b). To test if genetic deletion of CypD can prevent this social deficit, we
399 performed a social interaction and recognition task (Fig. 6F-G). Mice initially show great interest
400 anytime a new mouse is introduced into their home cage but gradually reduce their investigation
401 time with repeated exposures (trials 1-4). This can be used to investigate differences in baseline
402 social interaction and recognition memory when a new stimulus mouse is introduced into the
403 cage (trial 5). A two-way mixed ANOVA, revealed a significant main effect of treatment ($F_{(3, 32)}$ =
404 7.954, $p < 0.001$; Fig. 6G) on social interaction. Consistent with our previous reports

(Jeevakumar et al., 2015; Phensy et al., 2017b), WT-KET mice showed reduced investigation times across trials 1, 2, and 5. In contrast, *Ppif*$^{-/-}$-KET mice demonstrated investigation times similar to saline-treated controls across all five exposures, suggesting normal social interaction and recognition memory.

Discussion

NMDAR dysfunction disrupts normal development of GABAergic and glutamatergic networks and this may contribute to schizophrenia pathology (Krystal et al., 2002). Parvalbumin-expressing interneurons appear to be particularly susceptible to NMDAR dysfunction (Cohen et al., 2015), and changes in PVI and their synapses are well-documented in schizophrenia (Lewis et al., 2005; Nakazawa et al., 2012; Gonzalez-Burgos et al., 2015). PVI are highly sensitive to oxidative stress (Do et al., 2009), which can disrupt neuronal function and decrease NMDAR activity (Choi and Lipton, 2000). Mitochondria are the primary mediators of redox state (Rego and Oliveira, 2003; Bhatti et al., 2017) and they are abundant in PVI (Gulyas et al., 2006); however, their role in PVI dysfunction has received relatively little attention. Oxidative and other cellular stresses trigger translocation of CypD to the inner mitochondrial membrane, initiating formation of the mPTP (Baines et al., 2005). Prolonged mPTP formation leads to excessive levels of intracellular superoxide and pathological mitochondrial activity (Crompton, 2004; Lemasters et al., 2009). Glutamate excitotoxicity that results from overactivation of NMDA receptors and excessive calcium entry is a well-established initiator of chronic mPTP formation (Schinder et al., 1996).

NMDAR blockade disrupts development of PVI, alters E/I balance, and impairs cognitive performance (Wang et al., 2008; Jeevakumar and Kroener, 2016). There is strong evidence that these changes are mediated by oxidative stress (Radonjic et al., 2010; Powell et al., 2012), and we previously demonstrated that boosting antioxidant defense systems with N-acetyl cysteine can counter the physiological and behavioral deficits induced by perinatal KET-treatment (Phensy et al., 2017a). We also found that perinatal KET-treatment significantly increased levels of mitochondrial-derived ROS and reduced mitochondrial membrane potentials in PVI. These changes are signs of prolonged mPTP activation, suggesting mitochondria as important nodes in KET-induced PVI dysfunction. CypD is a necessary component of the mPTP, and reducing CypD translocation protects mitochondrial function (Du and Yan, 2010). Thus, we hypothesized that *Ppif*$^{-/-}$ mice would be protected from KET-induced increases in oxidative stress and PVI dysfunction.

We measured glutathione levels to determine the redox state of PFC tissue from adult KET- and SAL-treated mice. The ratio of GSH to GSSG indicates cell redox status, with healthy cells having a large GSH/GSSG ratio, that drops when they get exposed to oxidative stress (Pizzorno, 2014). Wildtype KET-treated mice showed a significant decrease in the GSH/GSSG ratio in PFC. This is in line with previous findings by us (Phensy et al., 2017a) and others (Powell et al., 2012) which have shown that NMDAR blockade during development drives oxidative stress in the frontal cortex. We also found increased levels of 4-HNE, a byproduct of lipid peroxidation, in prefrontal PVI of WT-KET mice. Lipid peroxidation occurs when free radicals damage lipids and it is an indicator of the damage that results from oxidative stress.

Ppif$^{-/-}$-KET mice demonstrated robust protection against KET-induced reductions in the GSH/GSSG ratio and the increase of 4-HNE levels in PVI (Figs 2,3). Because *Ppif*$^{-/-}$-KET mice also showed no significant loss of PV immunofluorescence in the PFC these results support the idea that PVI dysfunction results from mitochondrial oxidative stress. Previous reports have shown that PVI dysfunction following perinatal NMDAR blockade requires activation of NADPH-oxidase 2 (NOX2) (Behrens et al., 2007; Sorce et al., 2010). Interestingly, there is evidence for significant crosstalk between mitochondria and NOX2, which can reciprocally drive ROS production (Dikalov, 2011; Daiber et al., 2017). Thus, our data support these studies and suggest a complementary mechanism to NOX2-mediated PVI deficits.

NMDAR hypofunction in PVI is believed to contribute to aberrant synaptic activity in schizophrenia (Homayoun and Moghaddam, 2007). NMDARs can be directly inhibited by oxidizing agents via interaction on a redox-sensitive site on the receptor (Choi and Lipton, 2000). Developmental NMDAR blockade with ketamine leads to both long-lasting increases in oxidative stress and NMDAR-hypofunction in layer 2/3 prefrontal PVI (Phensy et al., 2017a). Because *Ppif*$^{-/-}$-KET mice exhibited reduced signs of oxidative stress, we investigated if this was accompanied by normal NMDAR function in layer 2/3 PVI. Consistent with our previous findings (Jeevakumar and Kroener, 2016; Phensy et al., 2017a), PVI in layers 2/3 from KET-treated WT mice showed reduced NMDAR currents. In contrast, *Ppif*$^{-/-}$-KET mice exhibited normal NMDAR:AMPAR current ratios (Figure 4). Because KET-treatment did not affect amplitudes of AMPA-mediated sEPSCs, this effect of CypD-deletion most likely represents a selective protection of NMDAR function. Reduced NMDAR activity has significant implications for PVI function. Gating of NMDARs causes influx of calcium which can help in persistent neuronal firing (Myme et al., 2003), an important feature of PVI physiology. Blocking NMDAR on PVI has been shown to impair the generation of gamma oscillations (Jadi et al., 2016), which are crucial to cognitive function (Fries, 2009; Sohal et al., 2009). Perturbations in gamma oscillations are believed to result from reduced PVI activity and a shift in the excitation/inhibition (E/I) balance (Gonzalez-Burgos et al., 2015; Sohal and Rubenstein, 2019). Consistent with the idea of a shift in the E/I balance, KET-treatment in WT mice lead to a long-lasting reduction in GABAergic inhibition at pyramidal neurons and increased glutamate release back onto layer 2/3 PVI. In contrast, in addition to preserved NMDAR function in PVI, *Ppif*$^{-/-}$ mice exhibited normal sEPSCs and mIPSCs in PVI and pyramidal cells, respectively, suggesting that normal E/I balance in the mPFC network was maintained.

Patients with schizophrenia suffer from a number of PFC-dependent cognitive deficits including disruptions in working memory, social cognition, attention, and cognitive flexibility (Braff et al., 1991; Gold et al., 1997; Nuechterlein et al., 2004). Evidence from clinical and preclinical models suggests that NMDAR hypofunction contributes to these deficits (Coyle, 2012; Cohen et al., 2015): NMDAR blockade can reduce cognitive abilities in healthy patients and exacerbate deficits in schizophrenia patients (Lahti et al., 1995; Malhotra et al., 1997; Krystal et al., 2002), and it impairs cognitive flexibility, episodic memory, and social interactions in rodents (Stefani and Moghaddam, 2005; Powell et al., 2012; Jeevakumar et al., 2015). In order to determine if CypD-deletion also protects against KET-induced cognitive deficits we examined the performance of *Ppif*$^{-/-}$-KET mice in a variety of tasks (Figure 6). In rodents, cognitive flexibility is most often assessed via attentional set-shifting tasks (Young et al., 2012). Here, we measured

cognitive flexibility through a rule-shifting task which requires only a simple shift from an egocentric response strategy to a visual cue-based strategy (Stefani and Moghaddam, 2005; Floresco et al., 2006). Consistent with previous findings (Stefani and Moghaddam, 2005; Broberg et al., 2008; Jeevakumar et al., 2015) we found that WT-KET mice required more trials to shift their strategies and committed a larger number of perseverative errors (Figure 6A-C). Perseverative errors suggest an inability to abandon a defunct strategy, a deficit that is frequently observed in patients with schizophrenia (Abbruzzese et al., 1996) or lesions of the PFC (Barcelo and Knight, 2002). Patients with schizophrenia also suffer from deficits in episodic memory (Ragland et al., 2009). In rodents, episodic memory can be assessed via the novel object recognition task. Performance on the task relies heavily on interactions between PFC and hippocampal circuits (Korotkova et al., 2010), which are disrupted by blockade (Jadi et al., 2016) or ablation (Korotkova et al., 2010) of NMDARs. Both acute (Rajagopal et al., 2014) and developmental (Jeevakumar et al., 2015; Phensy et al., 2017b) KET-treatment results in reduced novel object recognition. Finally, we examined changes in social interaction in KET-treated WT and *Ppif*$^{-/-}$ animals. Reduced social interactions and isolation are negative symptoms associated with schizophrenia (Millan et al., 2014; Green et al., 2015). Consistent with what we (Phensy et al., 2017b) and others (Powell et al., 2012) have previously shown, developmental NMDAR blockade in WT mice reduced social interaction times across all presentations of the stimulus mice. Importantly, *Ppif*$^{-/-}$ mice showed robust protection against all KET-induced behavioral deficits. These findings strongly suggest that transient NMDAR blockade affects cortical networks and behavior via processes that depend on proper mitochondrial function, and that modulation of the mPTP via genetic deletion of CypD can prevent these effects. These findings are in line with a number of other studies in which genetic deletion or pharmacological inhibition of CypD has been shown to offer protection against cognitive dysfunction in other preclinical disease models (Du et al., 2008; Yan et al., 2016; Nusrat et al., 2018). One previous study reported higher indices of anxiety and a reduced tendency to explore in *Ppif*$^{-/-}$ mice (Luvisetto et al., 2008); however, we did not find evidence for reduced exploration during NOR or the cross-maze rule-shifting task, nor did we observe any other unspecific phenotypical changes in *Ppif*$^{-/-}$ mice.

Taken together, our results underscore the impact of mitochondria on cortical networks and cognition. Mitochondria not only play essential roles in cell function, but their bioenergetics are crucial for proper neuronal development (Cobley, 2018), and even acute dysfunction impairs learning and memory (Mancini and Horvath, 2017). Here we illustrate how CypD activity can drive mitochondrial dysfunction in PVI and show that CypD may be a potential therapeutic target in protecting cognitive function in schizophrenia.

References

Abbruzzese M, Ferri S, Scarone S (1996) Performance on the Wisconsin Card Sorting Test in schizophrenia: perseveration in clinical subtypes. Psychiatry Res 64:27-33.

Abekawa T, Ito K, Nakagawa S, Koyama T (2007) Prenatal exposure to an NMDA receptor antagonist, MK-801 reduces density of parvalbumin-immunoreactive GABAergic neurons in the medial prefrontal cortex and enhances phencyclidine-induced hyperlocomotion but not behavioral sensitization to methamphetamine in postpubertal rats. Psychopharmacology 192:303-316.

Akbarian S, Huang HS (2006) Molecular and cellular mechanisms of altered GAD1/GAD67 expression in schizophrenia and related disorders. Brain research reviews 52:293-304.

Altar CA, Jurata LW, Charles V, Lemire A, Liu P, Bukhman Y, Young TA, Bullard J, Yokoe H, Webster MJ, Knable MB, Brockman JA (2005) Deficient hippocampal neuron expression of proteasome, ubiquitin, and mitochondrial genes in multiple schizophrenia cohorts. Biol Psychiatry 58:85-96.

Anticevic A, Gancsos M, Murray JD, Repovs G, Driesen NR, Ennis DJ, Niciu MJ, Morgan PT, Surti TS, Bloch MH, Ramani R, Smith MA, Wang XJ, Krystal JH, Corlett PR (2012) NMDA receptor function in large-scale anticorrelated neural systems with implications for cognition and schizophrenia. Proceedings of the National Academy of Sciences of the United States of America 109:16720-16725.

Baines CP, Kaiser RA, Purcell NH, Blair NS, Osinska H, Hambleton MA, Brunskill EW, Sayen MR, Gottlieb RA, Dorn GW, Robbins J, Molkentin JD (2005) Loss of cyclophilin D reveals a critical role for mitochondrial permeability transition in cell death. Nature 434:658-662.

Barcelo F, Knight RT (2002) Both random and perseverative errors underlie WCST deficits in prefrontal patients. Neuropsychologia 40:349-356.

Basso E, Fante L, Fowlkes J, Petronilli V, Forte MA, Bernardi P (2005) Properties of the permeability transition pore in mitochondria devoid of Cyclophilin D. The Journal of biological chemistry 280:18558-18561.

Behrens MM, Ali SS, Dao DN, Lucero J, Shekhtman G, Quick KL, Dugan LL (2007) Ketamine-induced loss of phenotype of fast-spiking interneurons is mediated by NADPH-oxidase. Science 318:1645-1647.

Belforte JE, Zsiros V, Sklar ER, Jiang Z, Yu G, Li Y, Quinlan EM, Nakazawa K (2010) Postnatal NMDA receptor ablation in corticolimbic interneurons confers schizophrenia-like phenotypes. Nat Neurosci 13:76-83.

Ben-Shachar D, Laifenfeld D (2004) Mitochondria, synaptic plasticity, and schizophrenia. International review of neurobiology 59:273-296.

Bhatti JS, Bhatti GK, Reddy PH (2017) Mitochondrial dysfunction and oxidative stress in metabolic disorders - A step towards mitochondria based therapeutic strategies. Biochim Biophys Acta Mol Basis Dis 1863:1066-1077.

Birnbaum R, Jaffe AE, Chen Q, Hyde TM, Kleinman JE, Weinberger DR (2015) Investigation of the prenatal expression patterns of 108 schizophrenia-associated genetic loci. Biological psychiatry 77:e43-51.

Birrell JM, Brown VJ (2000) Medial frontal cortex mediates perceptual attentional set shifting in the rat. The Journal of neuroscience : the official journal of the Society for Neuroscience 20:4320-4324.

Braff DL, Heaton R, Kuck J, Cullum M, Moranville J, Grant I, Zisook S (1991) The generalized pattern of neuropsychological deficits in outpatients with chronic schizophrenia with heterogeneous Wisconsin Card Sorting Test results. Arch Gen Psychiatry 48:891-898.

Braun I, Genius J, Grunze H, Bender A, Moller HJ, Rujescu D (2007) Alterations of hippocampal and prefrontal GABAergic interneurons in an animal model of psychosis induced by NMDA receptor antagonism. Schizophrenia research 97:254-263.

573 Broberg BV, Dias R, Glenthoj BY, Olsen CK (2008) Evaluation of a neurodevelopmental model of
574 schizophrenia--early postnatal PCP treatment in attentional set-shifting. Behav Brain Res
575 190:160-163.
576 Catts VS, Fung SJ, Long LE, Joshi D, Vercammen A, Allen KM, Fillman SG, Rothmond DA, Sinclair D, Tiwari
577 Y, Tsai SY, Weickert TW, Shannon Weickert C (2013) Rethinking schizophrenia in the context of
578 normal neurodevelopment. Frontiers in cellular neuroscience 7:60.
579 Chen Q, Vazquez EJ, Moghaddas S, Hoppel CL, Lesnefsky EJ (2003) Production of reactive oxygen species
580 by mitochondria: central role of complex III. The Journal of biological chemistry 278:36027-
581 36031.
582 Choi YB, Lipton SA (2000) Redox modulation of the NMDA receptor. Cell Mol Life Sci 57:1535-1541.
583 Cobley JN (2018) Synapse Pruning: Mitochondrial ROS with Their Hands on the Shears. Bioessays
584 40:e1800031.
585 Cohen SM, Tsien RW, Goff DC, Halassa MM (2015) The impact of NMDA receptor hypofunction on
586 GABAergic neurons in the pathophysiology of schizophrenia. Schizophr Res 167:98-107.
587 Connern CP, Halestrap AP (1994) Recruitment of mitochondrial cyclophilin to the mitochondrial inner
588 membrane under conditions of oxidative stress that enhance the opening of a calcium-sensitive
589 non-specific channel. The Biochemical journal 302 (Pt 2):321-324.
590 Coyle JT (2012) NMDA receptor and schizophrenia: a brief history. Schizophr Bull 38:920-926.
591 Crompton M (2004) Mitochondria and aging: a role for the permeability transition? Aging cell 3:3-6.
592 Daiber A, Di Lisa F, Oelze M, Kroller-Schon S, Steven S, Schulz E, Munzel T (2017) Crosstalk of
593 mitochondria with NADPH oxidase via reactive oxygen and nitrogen species signalling and its
594 role for vascular function. Br J Pharmacol 174:1670-1689.
595 Dikalov S (2011) Cross talk between mitochondria and NADPH oxidases. Free Radic Biol Med 51:1289-
596 1301.
597 Do KQ, Cabungcal JH, Frank A, Steullet P, Cuenod M (2009) Redox dysregulation, neurodevelopment,
598 and schizophrenia. Curr Opin Neurobiol 19:220-230.
599 Du H, Yan SS (2010) Mitochondrial medicine for neurodegenerative diseases. The international journal
600 of biochemistry & cell biology 42:560-572.
601 Du H, Guo L, Fang F, Chen D, Sosunov AA, McKhann GM, Yan Y, Wang C, Zhang H, Molkentin JD, Gunn-
602 Moore FJ, Vonsattel JP, Arancio O, Chen JX, Yan SD (2008) Cyclophilin D deficiency attenuates
603 mitochondrial and neuronal perturbation and ameliorates learning and memory in Alzheimer's
604 disease. Nat Med 14:1097-1105.
605 Floresco SB, Magyar O (2006) Mesocortical dopamine modulation of executive functions: beyond
606 working memory. Psychopharmacology 188:567-585.
607 Floresco SB, Ghods-Sharifi S, Vexelman C, Magyar O (2006) Dissociable roles for the nucleus accumbens
608 core and shell in regulating set shifting. J Neurosci 26:2449-2457.
609 Fries P (2009) Neuronal gamma-band synchronization as a fundamental process in cortical computation.
610 Annu Rev Neurosci 32:209-224.
611 Gold JM, Carpenter C, Randolph C, Goldberg TE, Weinberger DR (1997) Auditory working memory and
612 Wisconsin Card Sorting Test performance in schizophrenia. Arch Gen Psychiatry 54:159-165.
613 Gonzalez-Burgos G, Cho RY, Lewis DA (2015) Alterations in cortical network oscillations and parvalbumin
614 neurons in schizophrenia. Biol Psychiatry 77:1031-1040.
615 Green MF, Horan WP, Lee J (2015) Social cognition in schizophrenia. Nat Rev Neurosci 16:620-631.
616 Gulsuner S, Walsh T, Watts AC, Lee MK, Thornton AM, Casadei S, Rippey C, Shahin H, Consortium on the
617 Genetics of S, Group PS, Nimgaonkar VL, Go RC, Savage RM, Swerdlow NR, Gur RE, Braff DL, King
618 MC, McClellan JM (2013) Spatial and temporal mapping of de novo mutations in schizophrenia
619 to a fetal prefrontal cortical network. Cell 154:518-529.

620 Gulyas AI, Buzsaki G, Freund TF, Hirase H (2006) Populations of hippocampal inhibitory neurons express
621 different levels of cytochrome c. Eur J Neurosci 23:2581-2594.
622 Halestrap AP (2010) A pore way to die: the role of mitochondria in reperfusion injury and
623 cardioprotection. Biochemical Society transactions 38:841-860.
624 Hardingham GE, Do KQ (2016) Linking early-life NMDAR hypofunction and oxidative stress in
625 schizophrenia pathogenesis. Nat Rev Neurosci 17:125-134.
626 Harrison PJ, Owen MJ (2003) Genes for schizophrenia? Recent findings and their pathophysiological
627 implications. Lancet 361:417-419.
628 Hjelm BE, Rollins B, Mamdani F, Lauterborn JC, Kirov G, Lynch G, Gall CM, Sequeira A, Vawter MP (2015)
629 Evidence of Mitochondrial Dysfunction within the Complex Genetic Etiology of Schizophrenia.
630 Molecular neuropsychiatry 1:201-219.
631 Homayoun H, Moghaddam B (2007) NMDA receptor hypofunction produces opposite effects on
632 prefrontal cortex interneurons and pyramidal neurons. J Neurosci 27:11496-11500.
633 Hu W, Morris B, Carrasco A, Kroener S (2015) Effects of acamprosate on attentional set-shifting and
634 cellular function in the prefrontal cortex of chronic alcohol-exposed mice. Alcoholism, clinical
635 and experimental research 39:953-961.
636 Insel TR (2010) Rethinking schizophrenia. Nature 468:187-193.
637 Iwamoto K, Bundo M, Kato T (2005) Altered expression of mitochondria-related genes in postmortem
638 brains of patients with bipolar disorder or schizophrenia, as revealed by large-scale DNA
639 microarray analysis. Hum Mol Genet 14:241-253.
640 Jadi MP, Behrens MM, Sejnowski TJ (2016) Abnormal Gamma Oscillations in N-Methyl-D-Aspartate
641 Receptor Hypofunction Models of Schizophrenia. Biol Psychiatry 79:716-726.
642 Jeevakumar V, Kroener S (2016) Ketamine Administration During the Second Postnatal Week Alters
643 Synaptic Properties of Fast-Spiking Interneurons in the Medial Prefrontal Cortex of Adult Mice.
644 Cereb Cortex 26:1117-1129.
645 Jeevakumar V, Driskill C, Paine A, Sobhanian M, Vakil H, Morris B, Ramos J, Kroener S (2015) Ketamine
646 administration during the second postnatal week induces enduring schizophrenia-like behavioral
647 symptoms and reduces parvalbumin expression in the medial prefrontal cortex of adult mice.
648 Behav Brain Res 282:165-175.
649 Jiang Z, Cowell RM, Nakazawa K (2013) Convergence of genetic and environmental factors on
650 parvalbumin-positive interneurons in schizophrenia. Frontiers in behavioral neuroscience 7:116.
651 Kann O, Kovacs R (2007) Mitochondria and neuronal activity. American journal of physiology Cell
652 physiology 292:C641-657.
653 Korotkova T, Fuchs EC, Ponomarenko A, von Engelhardt J, Monyer H (2010) NMDA receptor ablation on
654 parvalbumin-positive interneurons impairs hippocampal synchrony, spatial representations, and
655 working memory. Neuron 68:557-569.
656 Krystal JH, Anand A, Moghaddam B (2002) Effects of NMDA receptor antagonists: implications for the
657 pathophysiology of schizophrenia. Arch Gen Psychiatry 59:663-664.
658 Lahti AC, Koffel B, LaPorte D, Tamminga CA (1995) Subanesthetic doses of ketamine stimulate psychosis
659 in schizophrenia. Neuropsychopharmacology 13:9-19.
660 Lemasters JJ, Theruvath TP, Zhong Z, Nieminen AL (2009) Mitochondrial calcium and the permeability
661 transition in cell death. Biochim Biophys Acta 1787:1395-1401.
662 Lewis DA, Hashimoto T, Volk DW (2005) Cortical inhibitory neurons and schizophrenia. Nat Rev Neurosci
663 6:312-324.
664 Lewis DA, Curley AA, Glausier JR, Volk DW (2012) Cortical parvalbumin interneurons and cognitive
665 dysfunction in schizophrenia. Trends in neurosciences 35:57-67.
666 Li Z, Okamoto K, Hayashi Y, Sheng M (2004) The importance of dendritic mitochondria in the
667 morphogenesis and plasticity of spines and synapses. Cell 119:873-887.

668 Luvisetto S, Basso E, Petronilli V, Bernardi P, Forte M (2008) Enhancement of anxiety, facilitation of
669 avoidance behavior, and occurrence of adult-onset obesity in mice lacking mitochondrial
670 cyclophilin D. Neuroscience 155:585-596.
671 Malhotra AK, Pinals DA, Adler CM, Elman I, Clifton A, Pickar D, Breier A (1997) Ketamine-induced
672 exacerbation of psychotic symptoms and cognitive impairment in neuroleptic-free
673 schizophrenics. Neuropsychopharmacology 17:141-150.
674 Mancini G, Horvath TL (2017) Mitochondria Bioenergetic and Cognitive Functions: The Cannabinoid Link.
675 Trends Cell Biol 27:391-392.
676 Millan MJ, Fone K, Steckler T, Horan WP (2014) Negative symptoms of schizophrenia: clinical
677 characteristics, pathophysiological substrates, experimental models and prospects for improved
678 treatment. Eur Neuropsychopharmacol 24:645-692.
679 Myme CI, Sugino K, Turrigiano GG, Nelson SB (2003) The NMDA-to-AMPA ratio at synapses onto layer
680 2/3 pyramidal neurons is conserved across prefrontal and visual cortices. J Neurophysiol 90:771-
681 779.
682 Nakazawa K, Zsiros V, Jiang Z, Nakao K, Kolata S, Zhang S, Belforte JE (2012) GABAergic interneuron
683 origin of schizophrenia pathophysiology. Neuropharmacology 62:1574-1583.
684 Nuechterlein KH, Barch DM, Gold JM, Goldberg TE, Green MF, Heaton RK (2004) Identification of
685 separable cognitive factors in schizophrenia. Schizophr Res 72:29-39.
686 Nusrat L, Livingston-Thomas JM, Raguthevan V, Adams K, Vonderwalde I, Corbett D, Morshead CM
687 (2018) Cyclosporin A-Mediated Activation of Endogenous Neural Precursor Cells Promotes
688 Cognitive Recovery in a Mouse Model of Stroke. Front Aging Neurosci 10:93.
689 Olney JW, Newcomer JW, Farber NB (1999) NMDA receptor hypofunction model of schizophrenia. J
690 Psychiatr Res 33:523-533.
691 Pers TH, Timshel P, Ripke S, Lent S, Sullivan PF, O'Donovan MC, Franke L, Hirschhorn JN, Schizophrenia
692 Working Group of the Psychiatric Genomics C (2016) Comprehensive analysis of schizophrenia-
693 associated loci highlights ion channel pathways and biologically plausible candidate causal
694 genes. Hum Mol Genet 25:1247-1254.
695 Phensy A, Driskill C, Lindquist K, Guo L, Jeevakumar V, Fowler B, Du H, Kroener S (2017a) Antioxidant
696 Treatment in Male Mice Prevents Mitochondrial and Synaptic Changes in an NMDA Receptor
697 Dysfunction Model of Schizophrenia. eNeuro 4.
698 Phensy A, Duzdabanian HE, Brewer S, Panjabi A, Driskill C, Berz A, Peng G, Kroener S (2017b) Antioxidant
699 Treatment with N-acetyl Cysteine Prevents the Development of Cognitive and Social Behavioral
700 Deficits that Result from Perinatal Ketamine Treatment. Front Behav Neurosci 11:106.
701 Pizzorno J (2014) Glutathione! Integr Med (Encinitas) 13:8-12.
702 Plitman E, Nakajima S, de la Fuente-Sandoval C, Gerretsen P, Chakravarty MM, Kobylianskii J, Chung JK,
703 Caravaggio F, Iwata Y, Remington G, Graff-Guerrero A (2014) Glutamate-mediated excitotoxicity
704 in schizophrenia: a review. Eur Neuropsychopharmacol 24:1591-1605.
705 Pocklington AJ, Rees E, Walters JT, Han J, Kavanagh DH, Chambert KD, Holmans P, Moran JL, McCarroll
706 SA, Kirov G, O'Donovan MC, Owen MJ (2015) Novel Findings from CNVs Implicate Inhibitory and
707 Excitatory Signaling Complexes in Schizophrenia. Neuron 86:1203-1214.
708 Powell SB, Sejnowski TJ, Behrens MM (2012) Behavioral and neurochemical consequences of cortical
709 oxidative stress on parvalbumin-interneuron maturation in rodent models of schizophrenia.
710 Neuropharmacology 62:1322-1331.
711 Prabakaran S, Swatton JE, Ryan MM, Huffaker SJ, Huang JT, Griffin JL, Wayland M, Freeman T, Dudbridge
712 F, Lilley KS, Karp NA, Hester S, Tkachev D, Mimmack ML, Yolken RH, Webster MJ, Torrey EF,
713 Bahn S (2004) Mitochondrial dysfunction in schizophrenia: evidence for compromised brain
714 metabolism and oxidative stress. Molecular psychiatry 9:684-697, 643.

715 Radonjic NV, Knezevic ID, Vilimanovich U, Kravic-Stevovic T, Marina LV, Nikolic T, Todorovic V,
716 Bumbasirevic V, Petronijevic ND (2010) Decreased glutathione levels and altered antioxidant
717 defense in an animal model of schizophrenia: long-term effects of perinatal phencyclidine
718 administration. Neuropharmacology 58:739-745.
719 Ragland JD, Laird AR, Ranganath C, Blumenfeld RS, Gonzales SM, Glahn DC (2009) Prefrontal activation
720 deficits during episodic memory in schizophrenia. Am J Psychiatry 166:863-874.
721 Rajagopal L, Massey BW, Huang M, Oyamada Y, Meltzer HY (2014) The novel object recognition test in
722 rodents in relation to cognitive impairment in schizophrenia. Curr Pharm Des 20:5104-5114.
723 Rajasekaran A, Venkatasubramanian G, Berk M, Debnath M (2015) Mitochondrial dysfunction in
724 schizophrenia: pathways, mechanisms and implications. Neurosci Biobehav Rev 48:10-21.
725 Rego AC, Oliveira CR (2003) Mitochondrial dysfunction and reactive oxygen species in excitotoxicity and
726 apoptosis: implications for the pathogenesis of neurodegenerative diseases. Neurochem Res
727 28:1563-1574.
728 Schinder AF, Olson EC, Spitzer NC, Montal M (1996) Mitochondrial dysfunction is a primary event in
729 glutamate neurotoxicity. The Journal of neuroscience : the official journal of the Society for
730 Neuroscience 16:6125-6133.
731 Sekar A, Bialas AR, de Rivera H, Davis A, Hammond TR, Kamitaki N, Tooley K, Presumey J, Baum M, Van
732 Doren V, Genovese G, Rose SA, Handsaker RE, Schizophrenia Working Group of the Psychiatric
733 Genomics C, Daly MJ, Carroll MC, Stevens B, McCarroll SA (2016) Schizophrenia risk from
734 complex variation of complement component 4. Nature 530:177-183.
735 Snyder MA, Gao WJ (2013) NMDA hypofunction as a convergence point for progression and symptoms
736 of schizophrenia. Front Cell Neurosci 7:31.
737 Sohal VS, Rubenstein JLR (2019) Excitation-inhibition balance as a framework for investigating
738 mechanisms in neuropsychiatric disorders. Mol Psychiatry 24:1248-1257.
739 Sohal VS, Zhang F, Yizhar O, Deisseroth K (2009) Parvalbumin neurons and gamma rhythms enhance
740 cortical circuit performance. Nature 459:698-702.
741 Sorce S, Schiavone S, Tucci P, Colaianna M, Jaquet V, Cuomo V, Dubois-Dauphin M, Trabace L, Krause KH
742 (2010) The NADPH oxidase NOX2 controls glutamate release: a novel mechanism involved in
743 psychosis-like ketamine responses. J Neurosci 30:11317-11325.
744 Stefani MR, Moghaddam B (2005) Transient N-methyl-D-aspartate receptor blockade in early
745 development causes lasting cognitive deficits relevant to schizophrenia. Biol Psychiatry 57:433-
746 436.
747 Steullet P, Cabungcal JH, Monin A, Dwir D, O'Donnell P, Cuenod M, Do KQ (2016) Redox dysregulation,
748 neuroinflammation, and NMDA receptor hypofunction: A "central hub" in schizophrenia
749 pathophysiology? Schizophr Res 176:41-51.
750 Steullet P, Cabungcal JH, Coyle J, Didriksen M, Gill K, Grace AA, Hensch TK, LaMantia AS, Lindemann L,
751 Maynard TM, Meyer U, Morishita H, O'Donnell P, Puhl M, Cuenod M, Do KQ (2017) Oxidative
752 stress-driven parvalbumin interneuron impairment as a common mechanism in models of
753 schizophrenia. Mol Psychiatry 22:936-943.
754 Timms AE, Dorschner MO, Wechsler J, Choi KY, Kirkwood R, Girirajan S, Baker C, Eichler EE, Korvatska O,
755 Roche KW, Horwitz MS, Tsuang DW (2013) Support for the N-methyl-D-aspartate receptor
756 hypofunction hypothesis of schizophrenia from exome sequencing in multiplex families. JAMA
757 Psychiatry 70:582-590.
758 Wang CZ, Yang SF, Xia Y, Johnson KM (2008) Postnatal phencyclidine administration selectively reduces
759 adult cortical parvalbumin-containing interneurons. Neuropsychopharmacology 33:2442-2455.
760 White RJ, Reynolds IJ (1996) Mitochondrial depolarization in glutamate-stimulated neurons: an early
761 signal specific to excitotoxin exposure. The Journal of neuroscience : the official journal of the
762 Society for Neuroscience 16:5688-5697.

763 Yan S, Du F, Wu L, Zhang Z, Zhong C, Yu Q, Wang Y, Lue LF, Walker DG, Douglas JT, Yan SS (2016) F1F0
764 ATP Synthase-Cyclophilin D Interaction Contributes to Diabetes-Induced Synaptic Dysfunction
765 and Cognitive Decline. Diabetes 65:3482-3494.
766 Young JW, Amitai N, Geyer MA (2012) Behavioral animal models to assess pro-cognitive treatments for
767 schizophrenia. Handb Exp Pharmacol:39-79.
768 Young JW, Powell SB, Risbrough V, Marston HM, Geyer MA (2009) Using the MATRICS to guide
769 development of a preclinical cognitive test battery for research in schizophrenia. Pharmacology
770 & therapeutics 122:150-202.
771 Zhang Z, Sun QQ (2011) Development of NMDA NR2 subunits and their roles in critical period
772 maturation of neocortical GABAergic interneurons. Developmental neurobiology 71:221-245.

773

774

775 **Figure legends:**

776

777 **Figure 1.** CypD-deletion (*Ppif*$^{-/-}$) protects against the loss of parvalbumin (PV) expression that
778 results from perinatal ketamine (KET) treatment. Wildtype (WT) or *Ppif*$^{-/-}$ mice received either
779 saline (SAL) or KET injections on postnatal days 7, 9, and 11. A) Representative confocal
780 images of PV immunofluorescence (red) and DAPI (blue) from layers 1-6 of adult medial
781 prefrontal cortex. B) Total PV-positive cells as a percentage of DAPI. Perinatal KET-treatment
782 significantly reduced PV expression in WT but not in *Ppif*$^{-/-}$ mice. Significance is indicated as *p
783 ≤ 0.05, and ***p ≤ 0.001, following Tukey correction.

784

785 **Figure 2.** CypD-deletion (*Ppif*$^{-/-}$) reduces perinatal ketamine (KET)-induced oxidative stress in
786 adult medial prefrontal cortex (mPFC). A) KET-treatment does not affect total glutathione levels.
787 B) KET-treatment significantly reduces the ratio of the reduced (GSH) over oxidized (GSSG)
788 form of glutathione in wildtype (WT) mice, indicating increased oxidative stress. KET-treated
789 *Ppif*$^{-/-}$ mice are protected from this shift in the GSH / GSSG ratio. C, D) Total levels of GSH (C)
790 and GSSG (D) in adult mPFC tissue. Significance is indicated as *p ≤ 0.05 and **p ≤ 0.01,
791 following Tukey correction.

792

793 **Figure 3.** Perinatal ketamine (KET)-treatment increases oxidative stress in parvalbumin-positive
794 interneurons (PVI) from wildtype (WT) but not from CypD knockout (*Ppif*$^{-/-}$) mice. A)
795 Representative confocal images of parvalbumin (PV, green) and 4-HNE (red)
796 immunofluorescence in the medial prefrontal cortex. B) PV cells in tissue from WT-KET mice
797 had significantly higher levels of 4HNE, a measure of lipid peroxidation and oxidative stress,
798 than saline-treated WT mice (WT-SAL). KET-treated *Ppif*$^{-/-}$ mice were protected from this
799 increase. Significance is indicated as *p ≤ 0.05, and **p ≤ 0.01, following Tukey correction.

800

801 **Figure 4.** CypD deletion (*Ppif*$^{-/-}$) protects against alterations in GABA release that develop in the
802 medial prefrontal cortex following perinatal ketamine (KET)-treatment. A) Representative traces
803 of miniature IPSCs (in tetrodotoxin) recorded in layer 2/3 pyramidal cells from in the 4 treatment
804 groups. B) Amplitude distribution of all mIPSC events in the 4 treatment groups. C) KET-
805 treatment significantly reduced the frequency, but not the amplitude of mIPSCs onto layer 2/3
806 pyramidal neurons from wildtype (WT) mice. Similar changes were not observed in *Ppif*$^{-/-}$-KET
807 mice. D) Representative traces of spontaneous IPSCs recorded in layer 2/3 pyramidal cells. E)
808 Amplitude distribution of all sIPSC events in the 4 treatment groups. F) KET-treatment did not
809 alter the frequency or amplitude of sIPSCs. Significance is indicated as *p ≤ 0.05, and **p ≤
810 0.01, following Tukey correction.

811

812 **Figure 5.** Perinatal ketamine (KET)-treatment alters glutamatergic transmission onto layer 2/3
813 parvalbumin-positive interneurons (PVI) in wildtype (WT), but not in CypD knockout (*Ppif*$^{-/-}$)
814 mice. A) Representative traces of NMDAR-currents (red) and AMPAR- (black) from GFP+ PVI

neurons in layers 2/3 of the medial prefrontal cortex. B) NMDAR:AMPAR ratios in the 4 treatment groups. Ketamine-treated WT mice exhibit markedly decreased NMDAR:AMPAR ratios compared to saline (SAL)-treated mice, as well as KET-treated *Ppif*$^{-/-}$ mice. C) Representative traces of spontaneous-EPSCs recorded at -70 mV. D) KET-treatment increased the frequency, but not the amplitude of sEPSCs in WT mice, but not in *Ppif*$^{-/-}$ mice. Significance is indicated as *p ≤ 0.05, and **p ≤ 0.01, following Tukey correction.

Figure 6. Perinatal ketamine (KET)-treatment induced behavioral deficits in wildtype (WT), but not in CypD knockout (*Ppif*$^{-/-}$) mice. A) Schematic overview of the Cross-Maze Rule Shifting task used to assess cognitive flexibility. Mice learn an egocentric strategy (Response Discrimination) in order to obtain a food reward and the next day are required to shift to a visual cue strategy (Shift to Visual Cue Day). B) All animals learned the initial response strategy at the same rate; however, WT-KET required a significantly larger number of trials to shift between strategies compared to saline-treated controls and KET-treated *Ppif*$^{-/-}$ mice. C) Error analysis based on error types committed during the Shift-to-Cue session. WT-KET animals show an increase in total errors and a significantly higher number of perseverative errors. D) Schematic overview of the setup used to test novel object recognition (NOR). E) KET-treatment reduced NOR in WT, but not in *Ppif*$^{-/-}$ mice. F) Test of social interaction and recognition. A stimulus mouse is placed in the home-cage of the test mouse for four 1-minute sessions (10-minute inter-trial-intervals) and social interaction time is recorded. On a fifth trial, a novel stimulus mouse is introduced to test social recognition. G) KET-treatment results in reduced interaction times across all sessions. *Ppif*$^{-/-}$-KET mice patterns of social interaction comparable to saline-treated controls. A-F: Significance is indicated as *p ≤ 0.05, **p ≤ 0.01, and ***p ≤ 0.001, following Tukey correction. G: Significance is indicated as*p ≤ 0.05 WT-SAL vs WT-KET, ***p ≤ 0.001 WT-SAL vs WT-KET, and +p ≤ 0.05 for WT-KET vs *Ppif*$^{-/-}$-KET following Tukey correction.

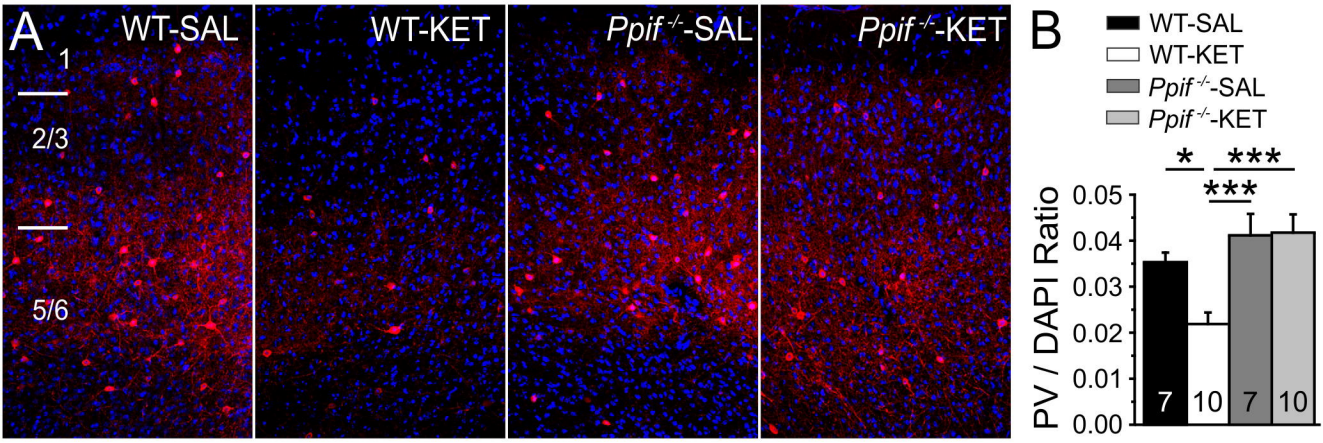
A
WT-SAL
WT-KET
Ppif -/--SAL
Ppif -/--KET
1
2/3
5/6
B
WT-SAL
WT-KET
Ppif -/--SAL
Ppif -/--KET
*
***
***
PV / DAPI Ratio
0.05
0.04
0.03
0.02
0.01
0.00
7
10
7
10

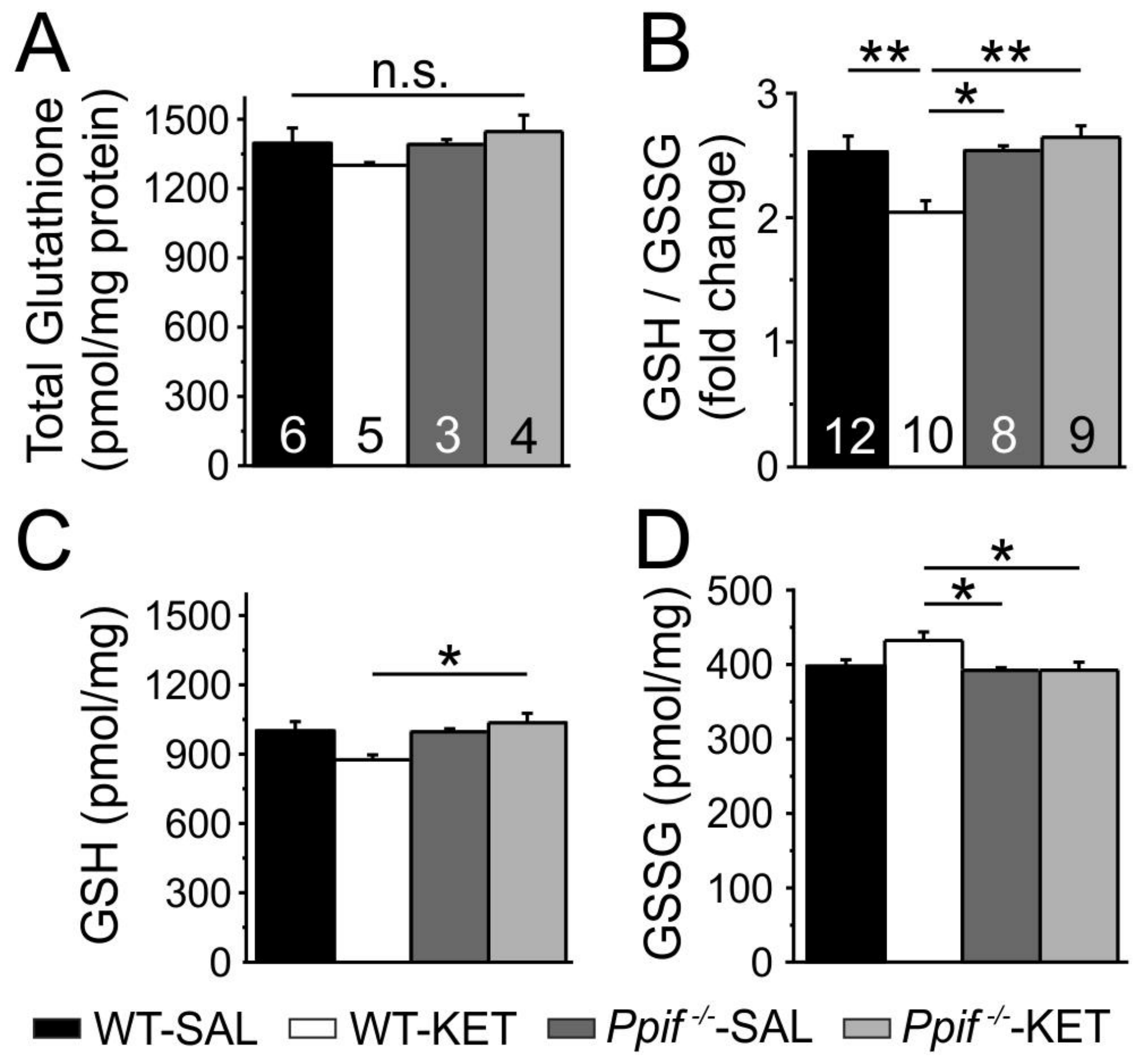
A
n.s.
Total Glutathione
(pmol/mg protein)
1500
1200
900
600
300
0
6
5
3
4
B
**
**
*
GSH / GSSG
(fold change)
3
2
1
0
12
10
8
9
C
*
GSH (pmol/mg)
1500
1200
900
600
300
0
D
*
*
GSSG (pmol/mg)
500
400
300
200
100
0
WT-SAL
WT-KET
Ppif -/--SAL
Ppif -/--KET

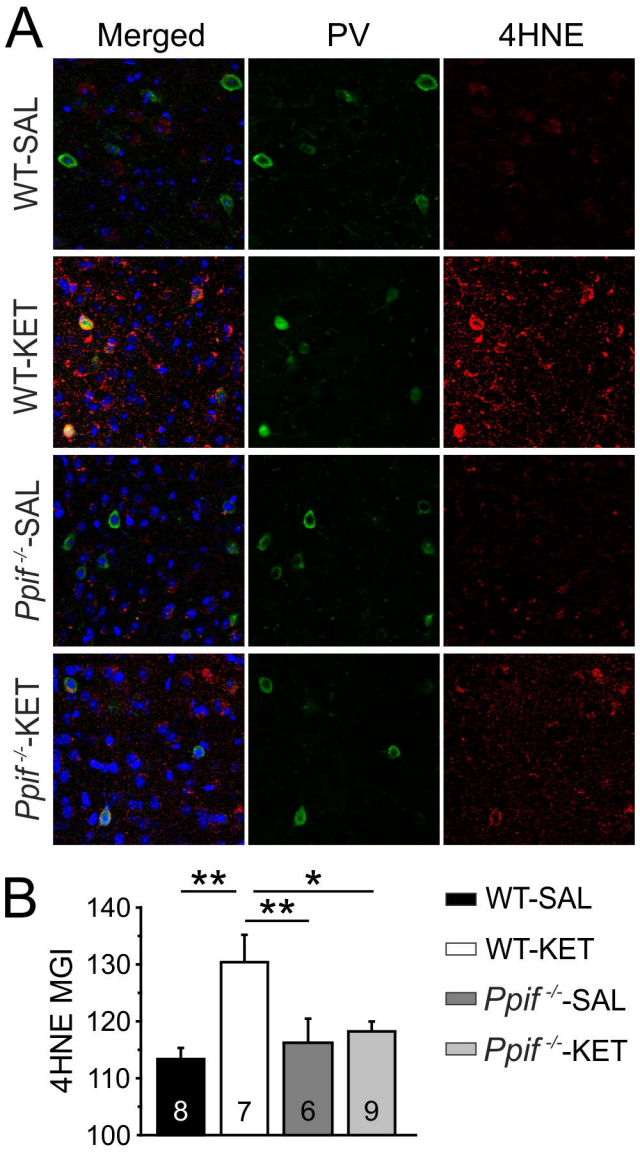
A
Merged
PV
4HNE
WT-SAL
WT-KET
Ppif -/--SAL
Ppif -/--KET
B
4HNE MGI
140
130
120
110
100
**
**
*
8
7
6
9
WT-SAL
WT-KET
Ppif -/--SAL
Ppif -/--KET

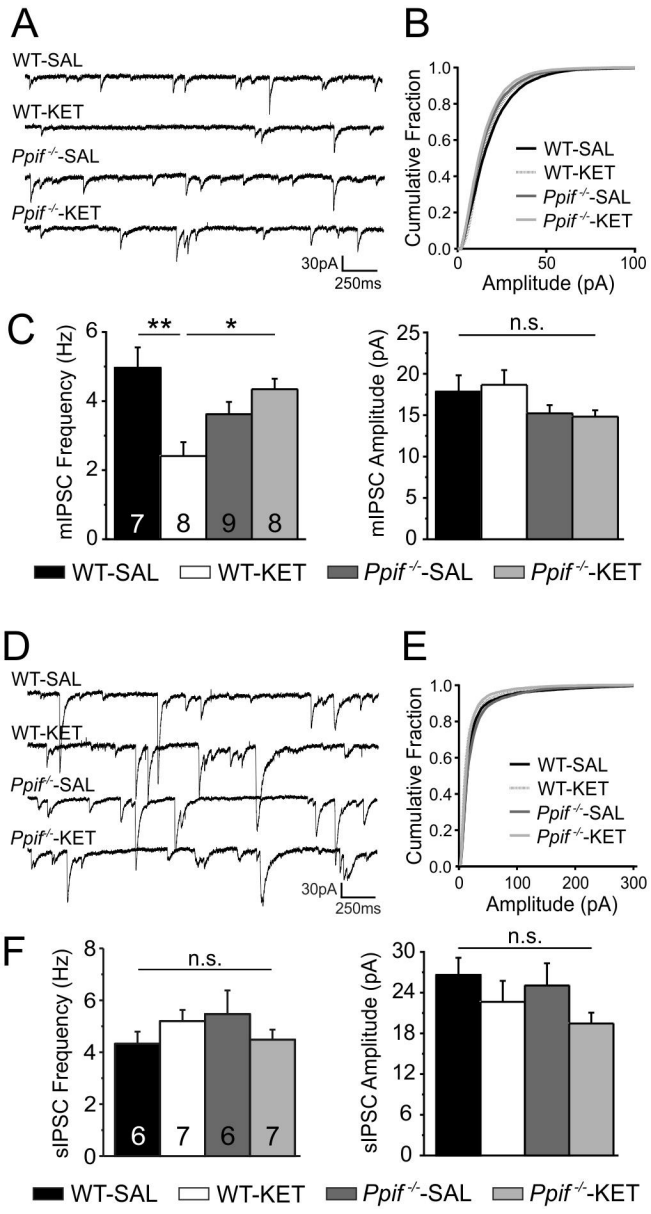
A
WT-SAL
WT-KET
Ppif-/--SAL
Ppif-/--KET
30pA
250ms
B
Cumulative Fraction
1.0
0.8
0.6
0.4
0.2
0.0
0
50
100
Amplitude (pA)
WT-SAL
WT-KET
Ppif-/--SAL
Ppif-/--KET
C
mIPSC Frequency (Hz)
6
4
2
0
**
*
7
8
9
8
mIPSC Amplitude (pA)
25
20
15
10
5
0
n.s.
WT-SAL
WT-KET
Ppif-/--SAL
Ppif-/--KET
D
WT-SAL
WT-KET
Ppif-/--SAL
Ppif-/--KET
30pA
250ms
E
Cumulative Fraction
1.0
0.8
0.6
0.4
0.2
0.0
0
100
200
300
Amplitude (pA)
WT-SAL
WT-KET
Ppif-/--SAL
Ppif-/--KET
F
sIPSC Frequency (Hz)
8
6
4
2
0
n.s.
6
7
6
7
sIPSC Amplitude (pA)
30
24
18
12
6
0
n.s.
WT-SAL
WT-KET
Ppif-/--SAL
Ppif-/--KET

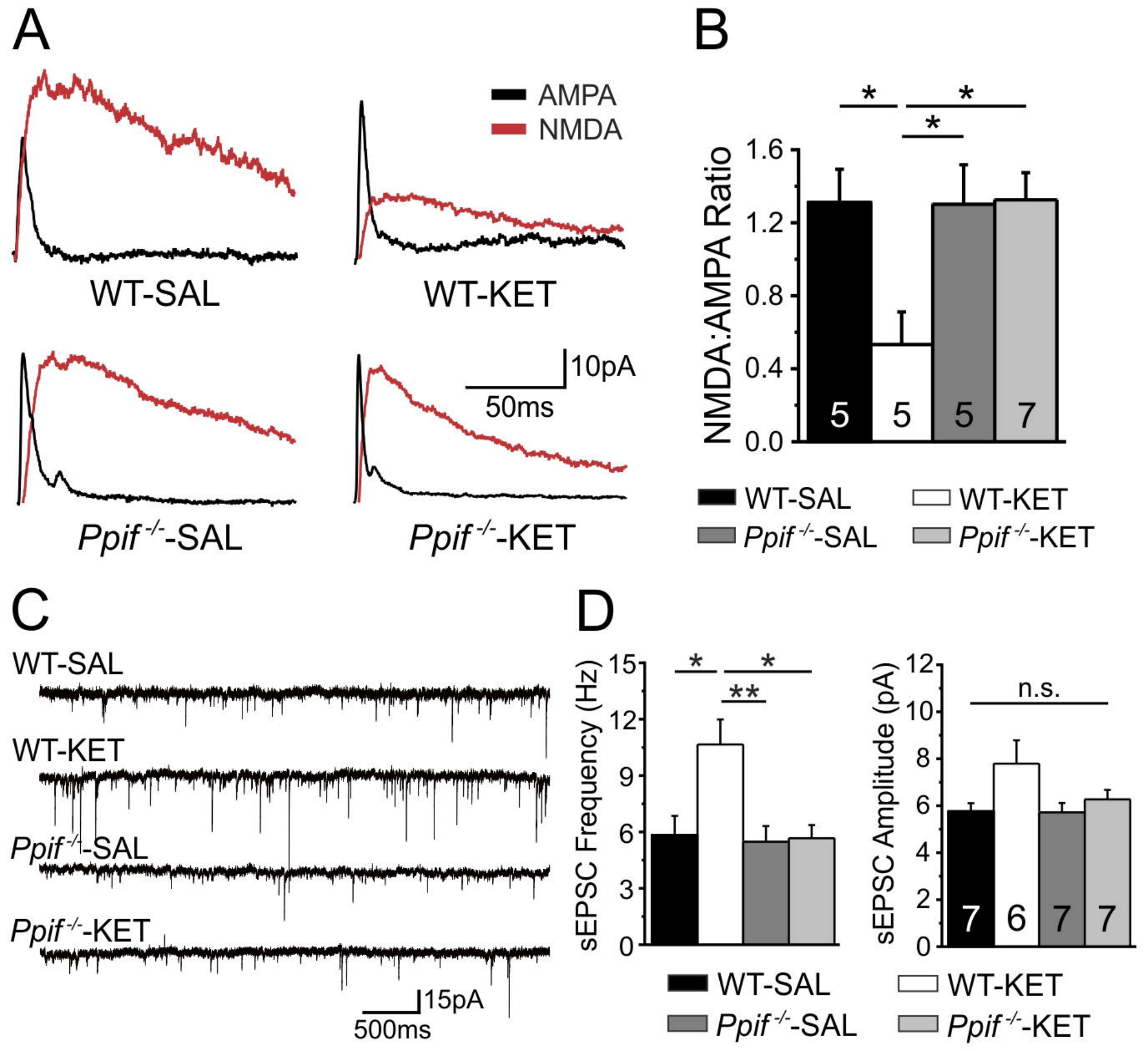
A
AMPA
NMDA
WT-SAL
WT-KET
10pA
50ms
Ppif -/--SAL
Ppif -/--KET
B
NMDA:AMPA Ratio
1.6
1.2
0.8
0.4
0.0
*
*
*
5
5
5
7
WT-SAL
WT-KET
Ppif -/--SAL
Ppif -/--KET
C
WT-SAL
WT-KET
Ppif -/--SAL
Ppif -/--KET
15pA
500ms
D
sEPSC Frequency (Hz)
15
12
9
6
3
0
*
*
**
sEPSC Amplitude (pA)
12
10
8
6
4
2
0
n.s.
7
6
7
7
WT-SAL
WT-KET
Ppif -/--SAL
Ppif -/--KET

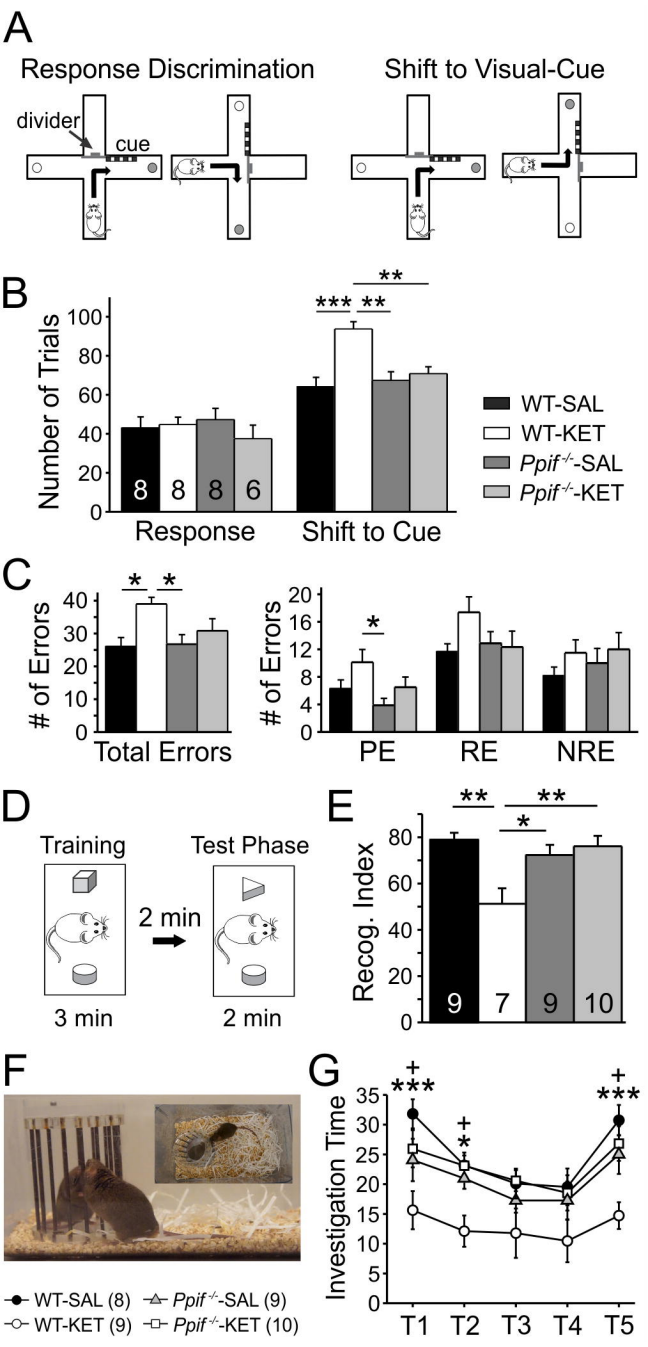
A
Response Discrimination
Shift to Visual-Cue
divider
cue
B
Number of Trials
WT-SAL
WT-KET
Ppif-/--SAL
Ppif-/--KET
8
8
8
6
Response
Shift to Cue
C
# of Errors
Total Errors
PE
RE
NRE
D
Training
Test Phase
2 min
3 min
2 min
E
Recog. Index
9
7
9
10
F
WT-SAL (8)
Ppif-/--SAL (9)
WT-KET (9)
Ppif-/--KET (10)
G
Investigation Time
T1
T2
T3
T4
T5